Available online at www.sciencedirect.com
ScienceDirect
Journal of Solid State Chemistry 181 (2008) 1285–1291
JOURNAL OF SOLID STATE CHEMISTRY
www.elsevier.com/locate/jssc

Electronic parameters of $Sr_2Nb_2O_7$ and chemical bonding

V.V. Atuchin[a,*], J.-C. Grivel[b], A.S. Korotkov[a], Zhaoming Zhang[c]

[a]*Laboratory of Optical Materials and Structures, Institute of Semiconductor Physics, SB RAS, 630090, Novosibirsk 90, Russia*
[b]*National Laboratory for Sustainable Energy, Materials Research Department, Technical University of Denmark, Frederiksborgvej 399, DK-4000 Roskilde, Denmark*
[c]*Australian Nuclear Science and Technology Organisation, Lucas Heights, NSW 2234, Australia*

Received 26 October 2007; received in revised form 19 January 2008; accepted 21 January 2008
Available online 16 February 2008

Abstract

X-ray photoelectron spectroscopy (XPS) measurements were carried out on a strontium pyroniobate ($Sr_2Nb_2O_7$) powder sample, which was synthesized using standard solid-state method. The binding energy (BE) differences between the O 1*s* and cation core levels, Δ(O–Nb) = BE(O 1*s*)–BE(Nb $3d_{5/2}$) and Δ(O–Sr) = BE(O 1*s*)–BE(Sr $3d_{5/2}$), were used to characterize the valence electron transfer on the formation of the Nb–O and Sr–O bonds. The chemical bonding effects were considered on the basis of our XPS results for $Sr_2Nb_2O_7$ and earlier published structural and XPS data for other Sr- or Nb-containing oxide compounds. The new data point for $Sr_2Nb_2O_7$ is consistent with the previously derived relationship for a set of Nb^{5+}-niobates that Δ(O–Nb) increases with increasing mean Nb–O bond distance, *L*(Nb–O). A new empirical relationship between Δ(O–Sr) and *L*(Sr–O) was also obtained. Interestingly, the correlation between Δ(O–Sr) and *L*(Sr–O) was found to differ from that between Δ(O–Nb) and *L*(Nb–O). Possible cause for the difference is discussed.

Keywords: X-ray photoelectron spectroscopy; $Sr_2Nb_2O_7$; Crystal structure; Chemical bonding

1. Introduction

Strontium pyroniobate ($Sr_2Nb_2O_7$) is a ferroelectric material with very high Curie temperature ($T_C = 1342\,^{\circ}C$), very high chemical and thermal stability, and remarkable piezoelectric and electro-optic properties [1–4]. The $Sr_2Nb_2O_7$ crystal structure is orthorhombic, in space $Cmc2_1$ [5,6]. The unit cell is quite large, with $a = 3.9544$, $b = 26.767$, and $c = 5.6961$ Å [6]. As shown in Fig. 1, the structure is formed by slabs (with a perovskite-type structure) parallel to (010) planes. There are two types of Nb atoms, both in octahedral position, with similar Nb–O distances in the range of 1.81–2.31 and 1.82–2.24 Å. There are also two types of Sr positions. The Sr(1) atom, lying near the boundary of the slab and linking adjacent slabs, is surrounded by seven oxygens at a distance 2.47–2.92 Å away (not counting the bonding with more distant oxygen atoms [6]). The Sr(2) atom is positioned inside the slab and coordinated to 12 oxygen atoms with a Sr–O distance in the range of 2.55–3.01 Å. The optical properties of $Sr_2Nb_2O_7$ include the presence of lightwave phase-matching for second-harmonic generation under pumping by Nd:YAG laser ($\lambda = 1064$ nm), noticeable nonlinear optical coefficients and very weak photorefractive effect due to high photoconductivity [7]. The dielectric constants of $Sr_2Nb_2O_7$ can be tuned effectively with doping by such metals as Ta, V, or La into the Sr or Nb crystal sites and these solid solutions are promising as working media in ferroelectric random access memory devices [8–12]. Recently, a technique has been proposed for the fabrication of $Sr_2Nb_2O_7$ nanorods, which enables further miniaturization of this piezoelectric material in electronic devices [13,14]. In addition, pure and N-doped $Sr_2Nb_2O_7$ are active photocatalysts for splitting water into H_2 and O_2 under ultraviolet and visible range illumination [15–17].

In order to utilize the effects mentioned above, it is important to have a thorough understanding of the chemical bonding in $Sr_2Nb_2O_7$. For potential applications such as electronic devices and catalysts, it is also necessary to determine the surface electronic parameters that control the chemical properties of the surface layer. One of the

*Corresponding author. Fax: +7 383 333 2771.
E-mail address: atuchin@thermo.isp.nsc.ru (V.V. Atuchin).

0022-4596/$ - see front matter © 2008 Elsevier Inc. All rights reserved.
doi:10.1016/j.jssc.2008.01.046

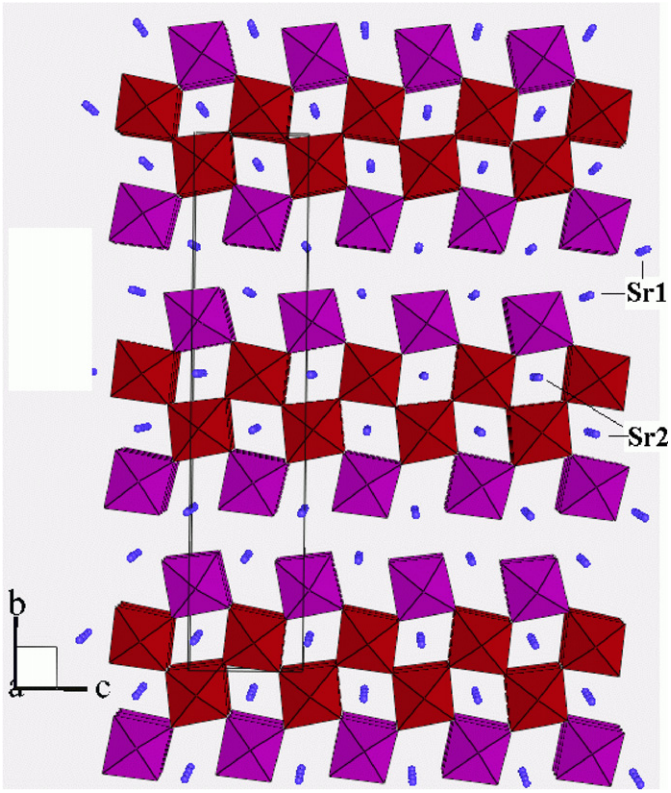

Fig. 1. Crystal structure of $Sr_2Nb_2O_7$ viewed along the *a*-axis. Small spheres and octagons represent Sr atoms and NbO_6 octahedra, respectively. The unit cell is outlined. In color version the Nb(1) and Nb(2) octagons are shown by red and violet, respectively.

most widely used methods for the characterization of surface electronic parameters is X-ray photoelectron spectroscopy (XPS), which can be used for quantitative determination of the electron charge transfer induced by the formation of chemical bonds [18]. A recent study on the N-doping effects in $Sr_2Nb_2O_7$-based solid solutions mentioned some XPS results, however no detailed analysis was provided [17]. The present study is aimed at producing a detailed XPS study of $Sr_2Nb_2O_7$ and to compare the Sr–O and Nb–O bonding in $Sr_2Nb_2O_7$ with other Sr- and Nb-bearing oxides. We will also search for any correlation between the electronic properties and chemical bonding in Sr- and Nb-bearing compounds.

2. Experimental

The starting reagents for sample preparation consisted of stoichiometric amounts of Nb_2O_5 (Aldrich, 99.99%) and $SrCO_3$ (Aldrich, >99.9%) powders. After grinding in an agate mortar, the mixture was calcined at 850 °C for 60 h and then sintered at $T = 1100$ °C for a total of 300 h (60 h + 90 h + 150 h) with intermediate grinding steps. The last heat treatment was performed without compaction, resulting in loosely agglomerated powders. This avoided the introduction of crystal lattice strain through grinding. X-ray diffraction (XRD) patterns were recorded after each heat treatment with an STOE diffractometer using Cu$K\alpha$ radiation. Cell parameter calculations were performed by a least-square fit method. Fig. 2 shows the XRD pattern recorded on the sample after the final heat treatment. Aside from three weak reflections attributed to the $Sr_5Nb_4O_{15}$ impurity phase, all lines correspond to the $Sr_2Nb_2O_7$ phase. None of the other phases reported in the $SrO–Nb_2O_5$ system was detected [19,20]. The calculated lattice parameters: $a = 3.9525(6)$ Å, $b = 26.780(4)$ Å, and $c = 5.7016(10)$ Å are in close agreement with those given in [21].

XPS analysis was performed in ultrahigh vacuum with a VG ESCALAB 220i-XL system employing a monochromatic Al$K\alpha$ (1486.6 eV) X-ray source. The X-ray gun was operated at 120 W, and the spectrometer pass energy was set at 20 and 100 eV for regional and survey scans, respectively. The powered sample was pressed onto a piece of freshly cleaved indium metal and mounted under a stainless steel foil with an open aperture of ~3 mm diameter. The diameter of the analysis area was approximately 500 μm, and the thickness of the probed surface layer was ~5 nm. A low-energy electron flood gun was used for the neutralization of surface charge buildup. The binding energies (BEs) were calibrated by fixing the saturated hydrocarbon component of the C 1*s* peak at 285.0 eV.

3. Results and discussion

The survey XPS spectrum recorded for $Sr_2Nb_2O_7$ is shown in Fig. 3. All peaks, except two, can be attributed to photoelectrons emitted from constituent element core levels. The line found at 285 eV is assigned to the C 1*s* core level, arising from adventitious hydrocarbons (due to exposure to air). A very weak peak around 458.3 eV was also detected and attributed to the small amount (<0.5 at%) of Ti impurity present in the sample presumably from the starting reagent $SrCO_3$. The Sr 3*d* and Nb 3*d* XPS spectra are shown in Figs. 4 and 5. Both doublets (due to spin–orbit splitting) show narrow symmetrical lines, confirming unique chemical states for Sr and Nb in the sample. Fig. 6 shows the O 1*s* core level. In this case, besides the dominant spectral component related to crystal oxygen, a higher BE shoulder is also evident. This smaller component is related to surface OH groups as well as adsorbed water (due to interaction of the oxide surface with water vapor in air). A set of representative core levels measured for $Sr_2Nb_2O_7$ is presented in Table 1. For comparison, the BE values of Nd 3*d* and O 1*s*, as estimated from Fig. 4 in Ref. [17], are also included in Table 1. A small BE shift by ~0.2–0.3 eV has been found between their BE values and those measured in our experiment, which is well within the acceptable range of experimental scatter in the results reported by different investigators. One other notable difference is the much narrower photoelectron peaks observed in our study (as indicated by full-widths at half-maximum (FWHM) in Table 1), probably largely due to the monochromatic X-ray source

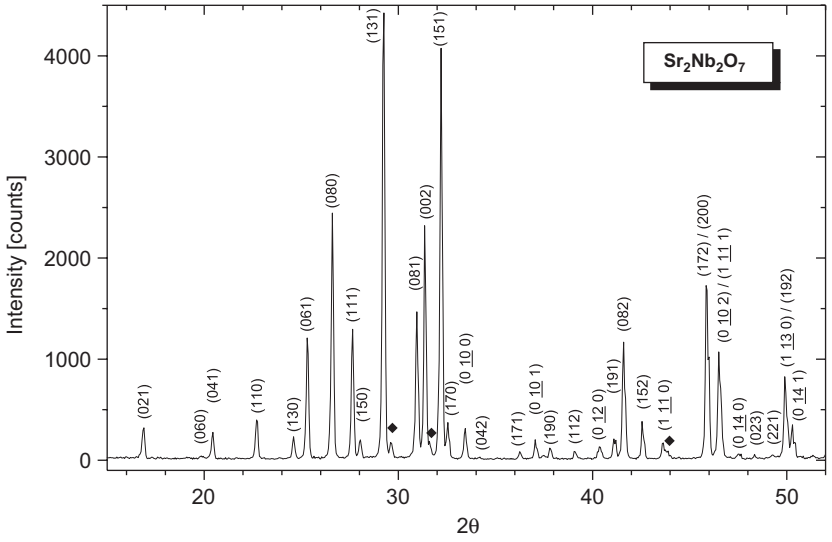

Fig. 2. The XRD pattern recorded on a powder sample of $Sr_2Nb_2O_7$. Diamonds denote reflections from the $Sr_5Nb_4O_7$ impurity phase.

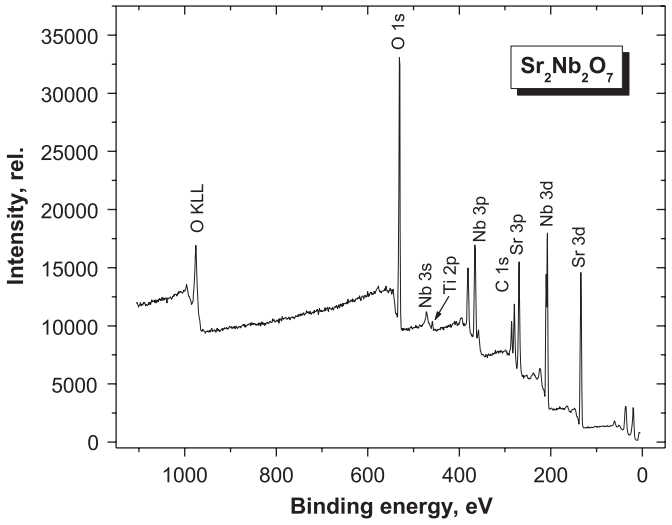

Fig. 3. Survey X-ray photoemission spectrum of $Sr_2Nb_2O_7$.

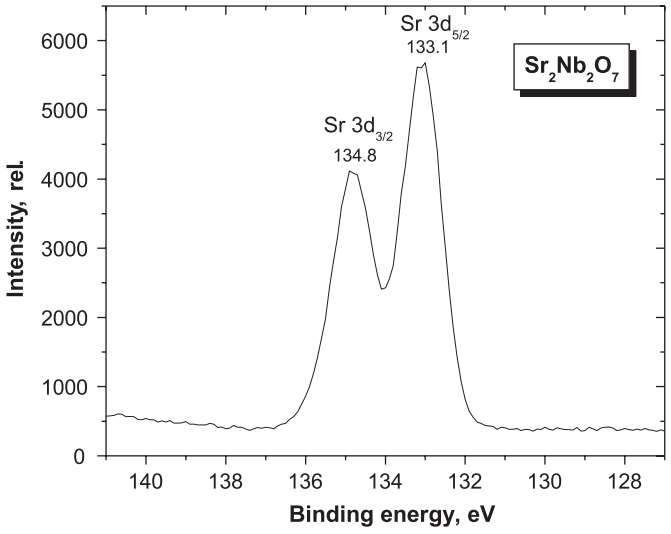

Fig. 4. Detailed XPS spectrum of the Sr 3*d* doublet from $Sr_2Nb_2O_7$.

employed by us, but also possibly due to the high quality of our sample.

It is well known that core level BE values can be used to obtain information on the chemical bonding in materials [18]. However, due to the uncertainties associated with absolute BE values (caused by different experimental conditions, e.g., charge Ref. [22]), chemical bonding effects in a compound can be better described by the BE difference, which is a more robust parameter as it is independent of absolute BE values. The advantage of using the BE difference has been demonstrated previously for different types of oxides [23–30]. For example, Δ(O–Nb) = BE(O 1*s*)–BE(Nb $3d_{5/2}$) was used successfully for the characterization of Nb–O bonding [25]. This quantitative parameter is independent of surface charging effects, and a correlation between Δ(O–Nb) and the mean chemical bond length *L*(Nb–O) was found for a set of niobates (all Nb surrounded by six O atoms) [25]. The Δ(O–Nb) versus *L*(Nb–O) plot from a group of Nb^{5+}-bearing niobates, as reported in Ref. [25], is reproduced here in Fig. 7 (solid squares). A general trend of increasing Δ(O–Nb) with increasing *L*(Nb–O) is evident in Fig. 7. As it appears, the increase in Δ(O–Nb), with increasing *L*(Nb–O), corresponds to a negative shift in the BE of Nb $3d_{5/2}$ core level together with a small positive change in the BE of O 1*s* core level. For $Sr_2Nb_2O_7$, the Δ(O–Nb) value was determined as 323.0 eV from our XPS results. According to the crystal structure data reported in Ref. [6], there are two Nb positions in the crystal lattice of $Sr_2Nb_2O_7$. Both Nb atoms are in octahedral coordination, surrounded by six oxygen atoms. The mean chemical bond length *L*(Nb–O) was derived from Ref. [6] as 200.3 pm, which is typical for Nb^{5+}-niobates. The relationship between Δ(O–Nb) and *L*(Nb–O) for $Sr_2Nb_2O_7$ was included in Fig. 7 (triangle).

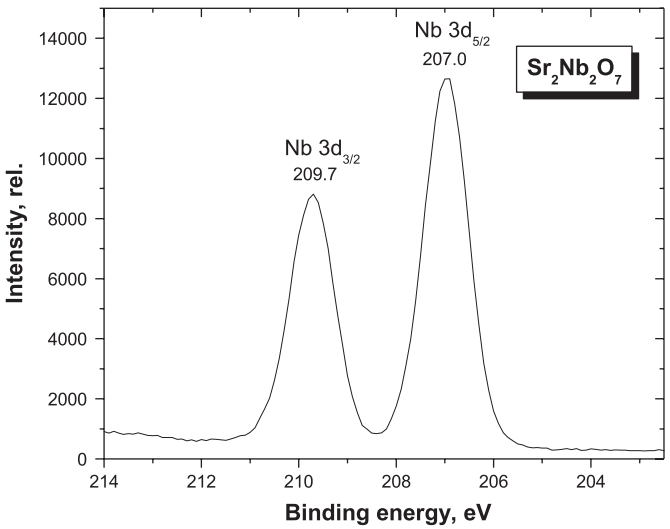

Fig. 5. Detailed XPS spectrum of the Nb 3*d* doublet from $Sr_2Nb_2O_7$.

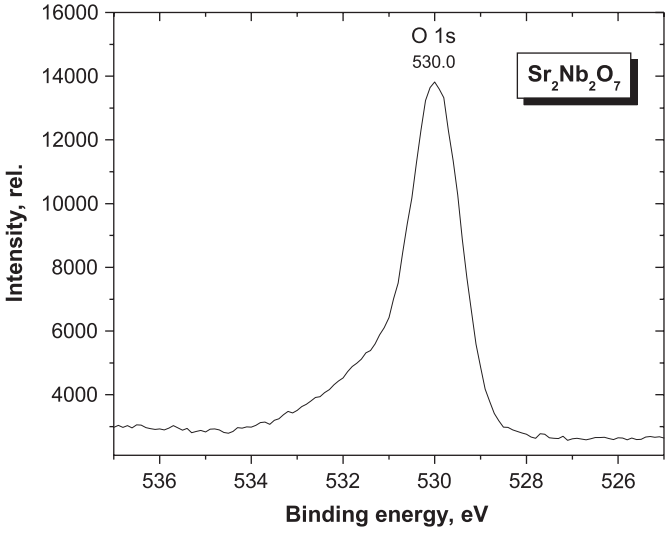

Fig. 6. Detailed XPS spectrum of the O 1*s* core level from $Sr_2Nb_2O_7$.

Table 1
Measured core level binding energy (BE) for $Sr_2Nb_2O_7$

Core level	BE (FWHM) (eV)	
	This study	[17][a]
Sr $3d_{5/2}$	133.1 (1.2)	–
Sr $3d_{3/2}$	134.8	–
Nb $3d_{5/2}$	207.0 (1.0)	206.7
Nb $3d_{3/2}$	209.7	209.5
Sr $3p_{3/2}$	268.9	–
Sr $3p_{1/2}$	279.3	–
C 1*s*	Fixed at 285.0 (1.4)	–
Nb $3p_{3/2}$	365.2	–
O 1*s*	530.0 (1.4)	529.8

Numbers in parentheses are the measured full-widths at half-maximum (FWHM).

[a]The BE values were estimated from Fig. 4, and the reference C 1*s* BE value was not specified in the paper.

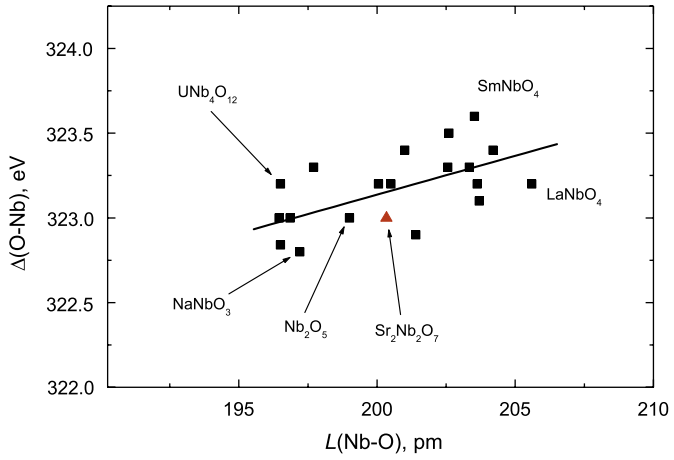

Fig. 7. Niobates on the plane of Δ(O–Nb)–L(Nb–O). Position of $Sr_2Nb_2O_7$ is shown by the solid circle. The solid squares denote data points of Nb^{5+}-niobates considered in Ref. [25]. The compounds defining the limits of Nb-bearing oxides are shown by formulas.

As seen, the data point for $Sr_2Nb_2O_7$ is in the middle of those for Nb^{5+}-niobates (Fig. 7), which means that the covalency of the Nb–O bonds in $Sr_2Nb_2O_7$ is intermediate in comparison with that observed in other Nb^{5+}-niobates [25].

To define the dependence of Δ(O–Sr) = BE(O 1*s*)–BE(Sr $3d_{5/2}$) on L(Sr–O) all available published results on the measurement of electronic parameters of Sr-bearing oxide crystals with XPS and related structural data were accumulated and compared. The collection of data is presented in Table 2 for 19 Sr-bearing oxide compounds. It should be mentioned that for SrO, $SrCO_3$, $SrSO_4$, $Sr(NO_3)_2$, and $SrTiO_3$ the BEs of element core levels were measured in several other studies as well [55–63]. The values of Δ(O–Sr) for SrO, $SrCO_3$, $SrSO_4$, $Sr(NO_3)_2$, and $SrTiO_3$ are in the range of 395.8–397.7 eV [32,55–58], 398.1–398.9 eV [32,55,57–59], 397.75–398.0 eV [32,59], 398.8–399.1 eV [32,55,59], and 396.5–397.1 eV [32,60–63], respectively. Such a scatter from different investigators of the same compound is not uncommon, due to differences in sample preparation and spectrometer calibration. To improve self-consistency, only the values reported in Ref. [32] were taken for the above-mentioned oxides, i.e., all the compounds were measured using the same spectrometer. The range of mean Sr^{2+}–O bond length listed in Table 2 is much wider than those found for Nb^{5+}–O [25] and Ti^{4+}–O [27], due to the variety of coordination number (6–12) exist for Sr-bearing oxides. It is well known that the Sr–O bond length increases with the coordination number [64]. Indeed, SrO (with six-coordinated Sr^{2+}) and $Na_2Sr(VO_3)_3$ and Sr_2CuO_3 (with eight-coordinated Sr^{2+}) define the lower limit of L(Sr–O), while the four compounds having 12-coordinated Sr^{2+} have the longest Sr–O bond distances ($SrTiO_3$, $Sr(NO_3)_2$, Sr_2FeMoO_6, and $SrSO_4$). In the case of $Sr_2Nb_2O_7$, the structure is more complex because there are

Table 2
Mean Sr–O bond distance (L(Sr–O)), Sr^{2+} coordination number and XPS results for Sr-bearing oxide crystals

Compound	L(Sr–O)		Coordination number	O 1s		Sr 3$d_{5/2}$		Δ(O–Sr)
	pm	Ref.		BE (eV)	Ref.	BE (eV)	Ref.	(eV)
SrO	258.0	[31]	6	530.0	[32]	132.6	[32]	397.4
$SrCO_3$	264.8	[33]	9	530.9	[32]	132.7	[32]	398.2
$SrSO_4$	283.7	[34]	12	531.6	[32]	133.85	[32]	397.75
$Sr(NO_3)_2$	277.65	[35]	12	532.8	[32]	134.0	[32]	398.8
$SrTiO_3$	275.7	[36]	12	529.0	[32]	132.5	[32]	396.5
$SrRuO_3$	265.0	[37]	8	528.7	p.c. [38]	132.0	p.c. [38]	396.7
$SrBPO_5$	272.6	[39]	10	531.3	[40]	132.5	[40]	398.8
$Na_2Sr(VO_3)_4$	257.2	[41]	8	530.2	[42]	133.0	p.c. [42]	397.2
$K_2Sr(VO_3)_4$	260.0	[41]	8	530.2	[42]	133.0	p.c. [42]	397.2
$Rb_2Sr(VO_3)_4$	259.4	[41]	8	530.2	[42]	133.0	p.c. [42]	397.2
$Cs_2Sr(VO_3)_4$	260.7	[41]	8	530.2	[42]	133.0	p.c. [42]	397.2
$SrLaAlO_4$	261.2	[43]	9	528.85	[44]	131.9	p.c. [44]	396.9
$SrLaGaO_4$	265.5	[45]	9	529.3	[46]	132.8	p.c. [46]	396.5
$SrPrAlO_4$	259.65	[47]	9	528.9	[48]	131.7	p.c. [48]	397.2
$SrPrGaO_4$	264.2	[49]	9	529.5	[50]	132.35	p.c. [50]	397.15
$SrMoO_4$	259.45	[51]	8	530.8	[52]	133.7	[52]	397.1
Sr_2FeMoO_6	279.3	[53]	12	529.2	p.c. [54]	132.9	p.c. [54]	396.3
Sr_2CuO_3	259.5	[65]	7	530.85	[66]	133.2	[66]	397.65
$Sr_2Nb_2O_7$	269.6	[6]	7 + 12	530.0	This study	133.1	This study	396.9

p.c.: private communication from the authors as well.

two types of Sr positions, the Sr(1) is coordinated by seven oxygens with L(Sr–O) = 260.9 pm and Sr(2) is coordinated by twelve oxygens with a relatively long L(Sr–O) = 278.3 pm distance. The mean Sr–O bond distance in $Sr_2Nb_2O_7$ sits, as expected, between those with nine and ten coordination numbers.

In Fig. 8, all the compounds listed in Table 2 are shown on the plane of Δ(O–Sr) versus L(Sr–O). Majority of the oxides show a Δ(O–Sr) within the range of 396.5–397.5 eV. Four compounds, $SrCO_3$, $SrBPO_5$, $Sr(NO_3)_2$, and $SrSO_4$, however, are characterized by much higher Δ(O–Sr) values, and therefore their corresponding data points are shifted away from the main cluster of points in Fig. 8. Nature of this deviation is not clear. But this anomaly might be related to the unique ligand groups in these compounds, which contain short covalent bonds between a non-metallic atom and oxygen (i.e., C–O, S–O, N–O, B–O, and P–O bonds). As shown, the $Sr_2Nb_2O_7$ data point is in the middle of the main cluster of Sr-bearing crystals on the Δ(O–Sr)–L(Sr–O) plane. From the main cluster of points, a general trend of decreasing Δ(O–Sr) with increasing L(Sr–O) can be observed. This is very intriguing as the trend is opposite to what was observed previously for Nb^{5+}-niobates [26] and Ti^{4+}-titanates [28]; Δ(O–Nb) and Δ(O–Ti) were found to increase with increasing L(Nb–O) and L(Ti–O), respectively. The exact cause for the observed difference is unclear. It is possible that the nature of the metal–oxygen bond governs the relationship between Δ(O–M) and L(M–O). The Sr–O chemical bonds are commonly classified as very ionic with complete transfer of valence electrons from Sr to O atoms. As a result, the BE of Sr 3$d_{5/2}$ line is not expected to change much in different

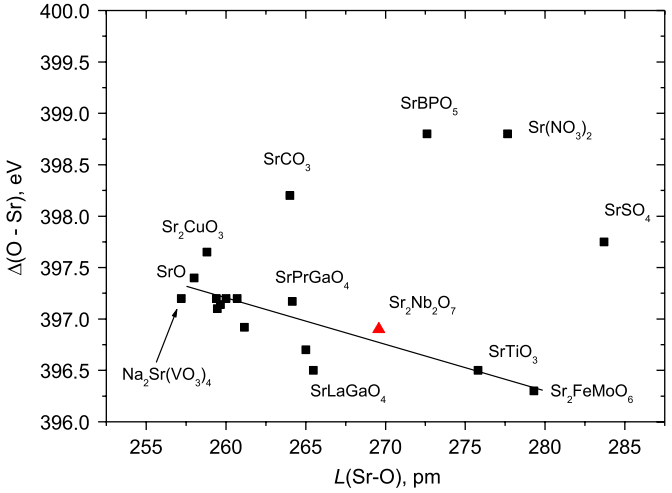

Fig. 8. Sr-bearing oxides (as listed in Table 2) on the plane of Δ(O–Sr)–L(Sr–O). The compounds defining the limits of Sr-bearing oxides are shown by formulas.

Sr-bearing oxides. Therefore, the decrease (or increase) of Δ(O–Sr) is predominantly determined by the decrease (or increase) in the O 1s BE value, which is in turn affected by the valence electron transfer from other cations that covalently bonded with oxygen. For example, the tetrahedrally coordinated Mo^{6+} and V^{5+} ions in $SrMoO_4$ and $M_2Sr(VO_3)_4$ (M = Na, K, Rb, and Cs) form relatively short and more covalent Mo–O and V–O bonds, resulting in higher O 1s BE values (i.e., higher Δ(O–Sr) values). On the other hand, the octahedrally coordinated Ti^{4+} and Mo^{5+} ions in $SrTiO_3$ and Sr_2FeMoO_6 form relatively long Ti–O and Mo–O bonds, leading to lower Δ(O–Sr) values.

In order to confirm this empirical relationship between Δ(O–Sr) and L(Sr–O), it is highly desirable to obtain XPS results from a larger number of Sr-bearing oxides, especially from clean single crystal surfaces, rather than those from less well defined powder surfaces (as quoted in this study). Nevertheless, the trend observed for Sr-bearing oxides in Fig. 8 is also expected for other oxides containing alkaline-earth and, probably, alkaline cations.

4. Conclusions

The $Sr_2Nb_2O_7$ powder was fabricated by solid-state synthesis and constituent element core levels were measured with XPS. Based on these experimental results and literature data (XPS and crystal structure) of other Sr- or Nb-containing oxide compounds, a qualitative relationship between the O and cation BE difference and the mean cation–oxygen bond distance was revealed on the planes of Δ(O–Nb)–L(Nb–O) and Δ(O–Sr)–L(Sr–O). The Δ(O–Nb) and L(Nb–O) values found for $Sr_2Nb_2O_7$ is consistent with those evaluated previously for a large set of Nb^{5+}-containing oxides, with increasing Δ(O–Nb) values upon the increase of Nb–O bond length, L(Nb–O). However, a relationship of decreasing Δ(O–Sr) with increasing L(Sr–O) was obtained for a set of Sr-bearing oxide crystals including $Sr_2Nb_2O_7$, which can not be explained by the simple ionic model. For more detailed observation of the Sr–O bonding in the future, it would be desirable to study a family of $Sr_2T_2O_7$ (T = V, Nb, and Ta) oxides with varied ionicity of the T–O bonds, and a set of different strontium niobates to see the effect of Sr/Nb variation on the values of Δ(O–Nb) and Δ(O–Sr) simultaneously.

Acknowledgments

The authors would like to thank Prof. Jungho Kim, Prof. M.N. Kuznetsov, Prof. A. Novosselov, and Prof. K. Kuepper who have provided us with unpublished XPS results and made this study more complete.

References

[1] Satoshi Nanamatsu, Masakazu Kimura, Kikuo Doi, Masao Takahashi, J. Phys. Soc. Jpn. 30 (1971) 300–301.
[2] M. Takahashi, S. Nanamatsu, M. Kimura, J. Cryst. Growth 13–14 (1972) 681–685.
[3] Satoshi Nanamatsu, Masakazu Kimura, Tsutomu Kawamura, J. Phys. Soc. Jpn. 38 (1975) 817–824.
[4] G. Shabbir, S. Kojima, J. Phys. D: Appl. Phys. 36 (2003) 1036–1039.
[5] N. Ishizawa, F. Marumo, T. Kawamura, M. Kimura, Acta Crystallogr. B31 (1975) 1912–1915.
[6] P. Daniels, R. Tamazyan, C.A. Kuntscher, M. Dressel, F. Lichtenberg, S. van Smaalen, Acta Crystallogr. B58 (2002) 970–976.
[7] S.S. Malhasian, S.Yu. Stefanovich, B.P. Nazarenko, M.F. Dubovik, Yu.N. Venevtsev, Cryst. Rep. 24 (1979) 518–523.
[8] Chang Young Kim, Chang Young Koo, Dong Chan Woo, Hee Young Lee, Jpn. J. Appl. Phys. 39B (2000) 5521–5524.
[9] Yoshikazu Fujimori, Naoki Izumi, Takashi Nakamura, Akira Kamisawa, Yasuhiro Shigematsu, Jpn. J. Appl. Phys. 36B (1997) 5935–5938.
[10] B. Brahmaroutu, G.L. Messing, S. Trolier-McKinstry, J. Mater. Sci. 35 (2000) 5673–5680.
[11] Toshiyuki Nakaiso, Minoru Noda, Masanori Okuyama, Jpn. J. Appl. Phys. 40B (2001) 2935–2939.
[12] Seana Seraji, Yun Wu, Steven Limmer, Tammy Chou, Caroyln Nguyen, Mike Forbess, G.Z. Cao, Mater. Sci. Eng. B88 (2002) 73–78.
[13] Steven J. Limmer, Seana Seraji, Yun Wu, Tammy P. Chou, Carolyn Nguyen, Guozhong Cao, Adv. Funct. Mater. 12 (2002) 59–64.
[14] Steven J. Limmer, Guozhong Cao, Adv. Mater. 15 (2003) 427–431.
[15] Hyun G. Kim, Dong W. Hwang, Jindo Kim, Young G. Kim, Jae S. Lee, Chem. Commun. (1999) 1077–1078.
[16] Akihiko Kudo, Hideki Kato, Seira Nakagawa, J. Phys. Chem. B104 (2000) 571–575.
[17] Sang Min Ji, Pramod H. Borse, Hyun Gyu Kim, Dong Won Hwang, Jum Suk Jang, Sang Won Bae, Jae Sung Lee, Phys. Chem. Chem. Phys. 7 (2005) 1315–1321.
[18] Paul S. Bagus, Francesc Illas, Gianfranco Pacchioni, Fulvio Parmigiani, J. Electron Spectrosc. Rel. Phenom. 100 (1999) 215–236.
[19] J.R. Carruthers, M. Grasso, J. Electrochem. Soc. 117 (1970) 1426–1430.
[20] P.P. Leshchenko, A.V. Shevchenko, L.N. Lykova, L.M. Kovba, E.A. Ippolitova, Izv. Akad. Nauk SSSR Neorg. Mater. 18 (1982) 1202–1205;
P.P. Leshchenko, A.V. Shevchenko, L.N. Lykova, L.M. Kovba, E.A. Ippolitova, Inorg. Mater. 18 (1982) 1013–1016 (Engl. Transl.).
[21] M. Mertens, J. Cooymans, ICDD Powder Diffraction File, Card number [52-321].
[22] P. Swift, Surf. Interface Anal. 4 (1982) 47–51.
[23] V.V. Atuchin, T. Hasanov, V.G. Kesler, A.E. Koch, L.D. Pokrovsky, Opt. Mater. 23 (2003) 385–392.
[24] V.V. Atuchin, V.G. Kesler, L.D. Pokrovsky, N.Yu. Maklakova, M. Yoshimura, N. Ushiyama, T. Matsui, K. Kamimura, Y. Mori, T. Sasaki, J. Korean Cryst. Growth Cryst. Technol. 13 (2003) 19–23.
[25] V.V. Atuchin, I.E. Kalabin, V.G. Kesler, N.V. Pervukhina, J. Elect. Spectrosc. Rel. Phenom. 142 (2005) 129–134.
[26] V.V. Atuchin, T.I. Grigorieva, I.E. Kalabin, V.G. Kesler, L.D. Pokrovsky, D.I. Shevtsov, J. Cryst. Growth 275 (2005) e1603–e1607.
[27] Victor V. Atuchin, Valery G. Kesler, Natalia V. Pervukhina, Zhaoming Zhang, J. Elect. Spectrosc. Rel. Phenom. 152 (2006) 18–24.
[28] V.V. Atuchin, O.A. Alekseeva, V.G. Kesler, L.D. Pokrovsky, N.I. Sorokina, V.I. Voronkova, J. Solid State Chem. 179 (2006) 2349–2355.
[29] V.V. Atuchin, V.G. Kesler, N.Yu. Maklakova, L.D. Pokrovsky, D.V. Sheglov, Eur. Phys. J. B51 (2006) 293–300.
[30] C.V. Ramana, V.V. Atuchin, U. Becker, R.C. Ewing, L.I. Isaenko, O.Yu. Khyzhun, A.A. Merkulov, L.D. Pokrovsky, A.K. Sinelnichenko, S.A. Zhurkov, J. Phys. Chem. C111 (2007) 2702–2708.
[31] D. Taylor, Trans. Br. Ceram. Soc. 83 (1984) 5–9.
[32] R.P. Vasquez, J. Electron Spectrosc. Rel. Phenom. 56 (1991) 217–240.
[33] D. Jaroch, G. Heger, Bull. Miner. 111 (1988) 139–142.
[34] M.A. Simonov, S.I. Troyanov, Geology 42 (1987) 77–79 (Vestnik Moscow University, Series 4).
[35] Hubert Nowotny, Gernot Heger, Acta Crystallogr. C39 (1983) 952–956.
[36] Yu.A. Abramov, V.G. Tsirel'son, V.E. Zavodnik, S.A. Ivanov, I.D. Brown, Acta Crystallogr. B51 (1995) 942–951.
[37] C.W. Jones, P.D. Battle, P. Lightfoot, W.T.A. Harrison, Acta Crystallogr. C45 (1989) 365–367.
[38] Jungho Kim, J.-Y. Kim, B.-G. Park, S.-J. Oh, Phys. Rev. B73 (2006) 235109.
[39] Shilie Pan, Yicheng Wu, Peixhen Fu, Guochun Zhang, Zhihua Li, Chenxia Du, Chuangtian Chen, Chem. Mater. 15 (2003) 2218–2221.
[40] B.V.R. Chowdari, G.V. Subba Rao, C.J. Leo, Mater. Res. Bull. 36 (2001) 727–736.
[41] V.G. Zubkov, A.P. Tyutyunnik, I.F. Berger, L.L. Surat, B.V. Slobodin, Z. Neorg. Khimii 48 (2003) 2074–2079.

[42] B.V. Slobodin, L.L. Surat, V.G. Zubkov, A.P. Tyutyunnik, I.E. Berger, M.V. Kuznetsov, L.A. Perelyaeva, I.R. Shein, A.L. Ivanovskii, Phys. Rev. B72 (2005) 155205.
[43] R.D. Shannon, R.A. Oswald, J.B. Parise, B.H.T. Chai, P. Byszewski, A. Pajaczkowska, R. Sobolewski, J. Solid State Chem. 98 (1) (1992) 90–98.
[44] A. Novosselov, A. Pajaczkowska, E. Talik, Cryst. Res. Technol. 36 (8–10) (2001) 859–864.
[45] James F. Britten, Hanna A. Dabkowska, Antoni B. Dabkowski, John L. Campbell, William J. Teesdale, Acta Crystallogr. C51 (1995) 1975–1977.
[46] A. Novosselov, A. Klos, E. Talik, A. Pajaczkowska, J. Electron Spectrosc. Rel. Phenom. 128 (2003) 129–133.
[47] T.M. Gesing, R. Uecker, J.-C. Buhl, Z. Kristallogr. NCS 214 (1999) 432.
[48] Andrei Novosselov, Ewa Talik, Anna Pajaczkowska, J. Alloys Compds. 351 (2003) 50–53.
[49] T.M. Gesing, R. Uecker, J.-C. Buhl, Z. Kristallogr. NCS 215 (2000) 14.
[50] Anna Pajaczkowska, Andrey Novoselov, Detlef Klimm, Ewa Talik, Reinhard Uecker, Cryst. Growth Des. 4 (2004) 497–501.
[51] A.K. Azad, S.-G. Eriksson, S.A. Ivanov, R. Mathieu, J. Svedlindh, H. Rundlof, J. Alloys Compds. 364 (2004) 77–82.
[52] V.I. Nefedov, M.N. Firsov, I.S. Shaplygin, J. Electron Spectrosc. Rel. Phenom. 26 (1982) 65–78.
[53] Anthony Arulraj, K. Ramesha, J. Gopalakrishnan, C.N.R. Rao, J. Solid State Chem. 155 (2000) 233–237.
[54] K. Kuepper, M. Kadiroğlu, A.V. Postnikov, K.C. Prince, M. Matteucci, V.R. Galakhov, H. Hesse, G. Borstel, M. Neumann, J. Phys.: Condens. Matter 17 (2005) 4309–4317.
[55] V. Young, T. Otagawa, Appl. Surf. Sci. 20 (1985) 228–248.
[56] Jean-Charles Dupin, Danielle Gonbeau, Philippe Vinatier, Alain Levasseur, Phys. Chem. Chem. Phys. 2 (2000) 1319–1324.
[57] P.A.W. van der Heide, Surf. Interface Anal. 33 (2002) 414–425.
[58] M.I. Sosulnikov, Yu.A. Teterin, J. Electron Spectrosc. Rel. Phenom. 59 (1992) 111–126.
[59] A.B. Christie, J. Lee, I. Sutherland, J.M. Walls, Appl. Surf. Sci. 15 (1983) 224–237.
[60] P.A.W. van der Heide, Q.D. Jiang, Y.S. Kim, J.W. Rabalais, Surf. Sci. 473 (2001) 59–70.
[61] P.A.W. van der Heide, Surf. Sci. 490 (2001) L619–L626.
[62] D. Kobayashi, H. Kumigashira, M. Oshima, T. Ohnishi, M. Lippmaa, K. Ono, M. Kawasaki, H. Koinuma, J. Appl. Phys. 96 (2004) 7183–7188.
[63] F. Amy, A. Wan, A. Kahn, F.J. Walker, R.A. McKee, J. Appl. Phys. 96 (2004) 1601–1606.
[64] R.D. Shannon, C.T. Prewitt, Acta Crystallogr. B25 (1969) 925–946.
[65] M.T. Weller, D.R. Lines, J. Solid State Chem. 82 (1989) 21–29.
[66] E.Z. Kurmaev, V.R. Galakhov, V.V. Fedorenko, L.V. Elokhina, S. Bartkowski, M. Neumann, C. Greaves, P.P. Edwards, M. Al-Mamouri, D.L. Novikov, Phys. Rev. 52 (4) (1995) 2390–2394.